e-ISSN: 2149-4584

Erzincan University Journal of Science and Technology

EJSAT 2025, 18 (3) 963-980

Research Article

Synthesis, X-ray Crystallography, Hirshfeld Surface, FT-IR, UV-Vis and DFT Studies of 2,6-Diaminopyridinium Saccharinate

Serkan GÜNEY [1*]

[1*] Ordu University, Ulubey Vocational Higher School, Ordu, Turkey

Received: 25/06/2025, **Revised:** 01/10/2025, **Accepted:** 16/10/2025, **Published:** 31/12/2025

Abstract

In this study, Density Functional Theory (DFT) was employed to explore the molecular geometry, vibrational behavior (FT-IR, UV-Vis spectra), and electronic features (HOMO–LUMO energy levels) of 2,6-diaminopyridinium saccharinate (HDAPYSAC). Computational studies were performed using the B3LYP exchange–correlation functional in conjunction with the 6–311G(d,p) basis set. Structural data obtained from single-crystal X-ray diffraction confirmed that HDAPYSAC, consisting of saccharinate and diaminopyridinium moieties, crystallizes in the orthorhombic crystal system and belongs to the *Fdd2* space group. To further investigate the nature of intermolecular interactions and electron density distribution, Hirshfeld surface mapping and two-dimensional fingerprint plot analyses were carried out. The most significant intermolecular contacts were H···H (32.5%), H···O/O···H (31.7%), H···C/C···H (16.5%), H···N/N···H (7.4%), C···C (5.5%), C···O/O···C (3.0%), and C···N/N···C (2.6%). The calculated HOMO–LUMO energy gap of 3.5661 eV indicates a stable molecular structure. UV–Visible spectroscopy revealed six distinct absorption bands at 276.33, 211.26, 200.10, 173.21, 164.35, and 163.62 nm, corresponding to indirect and direct transition energies of 36188, 47335, 49975, 57733, 60846, and 61117 cm^{-1}, respectively.

Keywords: FT-IR, UV-Vis, Crystal structure, Hirshfeld surface analysis

2,6-Diaminopiridinyum Sakkarinatın Sentezi, X-ışını Kristalografisi, Hirshfeld Yüzey Analizi, FT-IR, UV-Vis ve DFT Çalışmaları

Öz

Bu çalışmada, 2,6-diaminopiridinyum sakkarinat (HDAPYSAC) bileşiğinin moleküler yapısı, titreşimsel özellikleri (FT-IR, UV-Vis) ve elektronik özellikleri (HOMO–LUMO enerji seviyeleri), Yoğunluk Fonksiyonel Teorisi (DFT) kapsamında B3LYP/6–311G(d,p) teorik düzeyinde araştırılmıştır. Sakkarinat ve diaminopiridinyum alt birimlerinden oluşan HDAPYSAC molekülü, ortorombik kristal sisteminde ve *Fdd2* uzay grubunda kristalleşmiştir. Moleküller arası etkileşimler ve elektron yoğunluğu dağılımı, Hirshfeld yüzeyi ve parmak izi analizleriyle değerlendirilmiştir. En belirgin temaslar H···H (%32.5), H···O/O···H (%31.7), H···C/C···H (%16.5), H···N/N···H (%7.4), C···C (%5.5), C···O/O···C (%3.0) ve C···N/N···C (%2.6) olarak hesaplanmıştır. HOMO–LUMO enerji aralığı 3.5661 eV olarak bulunmuş ve bu durum bileşiğin kararlı yapıda olduğunu göstermektedir. UV–görünür bölge spektroskopisi ile yapılan optik analizlerde, bileşiğin 276.33, 211.26, 200.10, 173.21, 164.35 ve 163.62 nm dalga boylarında altı belirgin absorpsiyon bandı gösterdiği ve bu bantlara karşılık gelen dolaylı ve doğrudan geçiş enerji değerlerinin sırasıyla 36188, 47335, 49975, 57733, 60846 ve 61117 cm^{-1} olduğu belirlenmiştir.

Anahtar Kelimeler: FT-IR, UV-Vis., Kristal yapı, Hirshfeld yüzey analizi

*Corresponding Author: serkanguney@odu.edu.tr

Cite this Article: Erzincan University Journal of Science and Technology 2025, 18(3) 963-979.
https://doi.org/10.18185/erzifbed.172743

1. Introduction

Saccharin ($C_7H_5NO_3S$), one of the earliest artificial sweeteners, has garnered significant attention due to its zero-calorie content and remarkable stability under diverse conditions. Its versatility has facilitated its widespread use across various industries, particularly in the food and pharmaceutical sectors, where it is often employed in the form of water-soluble salts, such as sodium saccharin ($Na(sac)\cdot 2H_2O$). The saccharinate anion ($C_7H_4NO_3S^-$), formed through the deprotonation of saccharin, demonstrates exceptional coordination behavior with numerous metal cations, resulting in the formation of ionic saccharinates [1]. Owing to their structural versatility and multifunctional properties, these complexes have been widely investigated for potential roles in catalysis, materials development, and biomedical research [2, 3]. The unique ability of saccharinate to act as a multifunctional ligand is particularly noteworthy. It coordinates through various donor sites, including sulfonyl oxygen and nitrogen atoms, making it an attractive candidate for the design of novel coordination complexes. Structural analyses of various metal saccharinates, such as $Na(sac)\cdot 2/3H_2O$, $K(sac)\cdot 2/3H_2O$, and $Mg(sac)_2\cdot 7H_2O$, have revealed their broad structural adaptability and functional properties [4-6]. In contrast, non-metallic saccharinate salts are relatively rare, with $NH_4(sac)$ [7] and piperazinium disaccharinate, $(H_2ppz)(sac)_2$ [8], being among the few reported examples.

Recently, the focus has shifted towards hybrid organic-inorganic complexes, driven by their unique physicochemical properties and potential applications in crystal engineering and functional materials. Pyridinium-based cations, particularly 2,6-diaminopyridinium, have emerged as promising candidates for the development of innovative coordination compounds. These cations offer additional hydrogen-bonding capabilities, enhancing the stability and dimensionality of saccharinate complexes, and broadening their applicability in supramolecular chemistry [9-11]. Hybrid organic–inorganic complexes have been explored for applications in non-linear optics [12], gas storage and sensing [13], catalysis, and as proton conductors [14], underlining their multifunctionality in advanced material science.

In addition, several recent studies (2022–2024) have reported new saccharin derivatives and their complexes, highlighting their potential roles in supramolecular assemblies, functional materials, and biomedical applications [3, 15].

The synthesis, characterization, and biomedical applications of mixed-ligand metal saccharin complexes represent an intriguing area of study. In this work, we aimed to synthesize a mixed-ligand Zn(II) saccharinate complex containing 2,6-diaminopyridine. However, the 2,6-diaminopyridinium saccharinate compound was obtained instead. A detailed characterization of the compound's molecular and structural properties was accomplished through elemental analysis, FT-IR spectroscopy, and single-crystal X-ray diffraction methods.

The results provide valuable insights into the structural versatility of saccharinate-based systems and their potential for the development of functional materials.

2. Materials and Methods

2.1. Materials

All reagents were sourced from commercial vendors and used directly without undergoing any further purification steps. The precursor complex $[Zn(sac)_2(H_2O)_4]\cdot 2H_2O$ was synthesized following the procedures reported in the literature [16].

2.2. Synthesis

The compound 2,6-diaminopyridinium saccharinate (HDAPYSAC) was unexpectedly obtained as the main product during the reaction between $[Zn(sac)_2(H_2O)_4]\cdot 2H_2O$ and 2,6-diaminopyridine (dapy). Although the original goal of the experiment was to synthesize a zinc-saccharinate complex incorporating the dapy ligand, the reaction led instead to the isolation of HDAPYSAC.

For the synthesis of the target compound, dapy (0.218 g, 2.0 mmol) was first dissolved in 10 cm^3 of a methanol–isopropanol mixture (1:1, v/v). This solution was then gradually introduced into a magnetically stirred solution of tetraaquabis(saccharinato)zinc(II) dihydrate (0.538 g, 1 mmol) in 30 cm^3 of the same solvent mixture at ambient temperature. After mixing, the reaction was allowed to proceed without disturbance under room conditions for 24 hours. Upon completion, colorless crystals of the product were obtained, as illustrated in Figure 1. Elemental analysis for $C_{12}H_{12}N_4O_3S$ (292.32) yielded the following results: calculated C 49.95%, H 4.21%, N 19.23%, S 10.67%; found C 49.31%, H 4.14%, N 19.17%, S 10.97%.

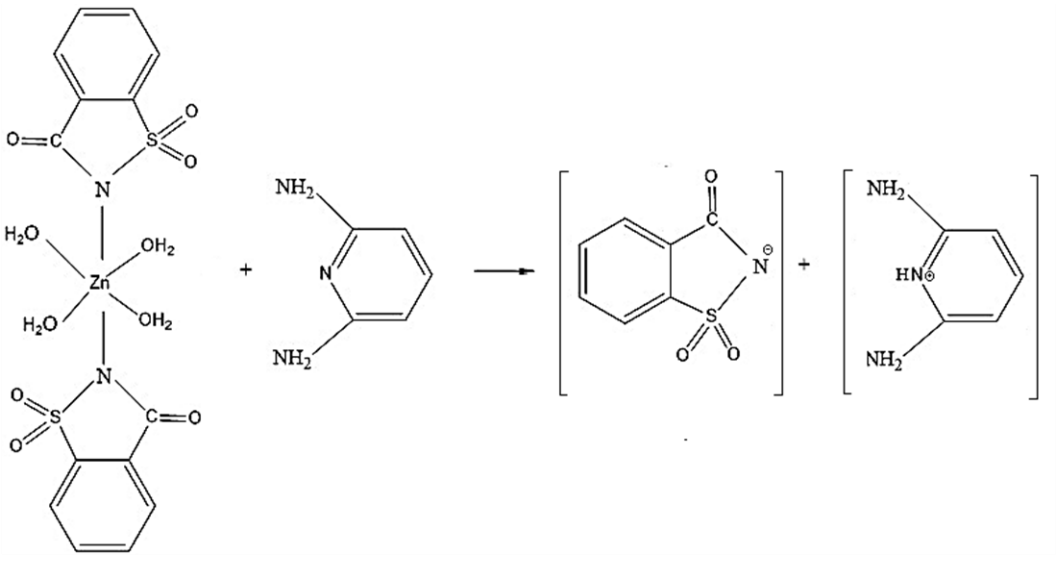

Figure 1. Synthesis scheme of HDAPYSAC

2.3. Physical Measurements

The molecular structure of HDAPYSAC was identified using single-crystal X-ray diffraction. The diffraction data were gathered using a STOE IPDS 2 diffractometer with graphite- X-ray intensity data were collected using monochromatic MoKα radiation (λ = 0.71073 Å) at 296 K [17]. Absorption corrections were carried out using equivalent reflections. Hydrogen atoms were placed in idealized positions and refined using a riding model with bond lengths constrained to 0.93 Å for C—H, 0.82 Å for O—H, and 0.86 Å for N—H. Isotropic displacement parameters were assigned as 1.2Ueq for carbon and nitrogen atoms and 1.5Ueq for oxygen atoms. The structure was solved and refined using the SHELXT-2018/3 program [18]. Molecular graphics were rendered with Mercury for Windows [19], and hydrogen bonding interactions were analyzed using the PLATON software [20]. The crystallographic data were prepared for publication using WinGX [21] and PublCIF [22].

Quantum chemical computations based on DFT were carried out with the Gaussian 09 software package [23], and molecular structures were visualized using GaussView 5.0 [24]. Calculations were performed using the B3LYP method, combining Becke's three-parameter exchange functional [25] and the Lee–Yang–Parr correlation functional [26] with the 6–311G(d,p) basis set.

The intermolecular interactions of the HDAPYSAC molecule were further investigated using Hirshfeld surface (HS) analysis implemented in the CrystalExplorer 17.5 software [27].

Elemental composition (C, H, N, and S) was assessed using a Vario Micro Cube Elemental Analyzer. The FT-IR spectrum was obtained using a Shimadzu IR Affinity-1 spectrophotometer within the range of 4000–300 cm^{-1}.

3. Findings and Discussion

3.1. Crystallography studies, molecular geometry, and structural parameters

Single-crystal X-ray analysis revealed that the compound crystallizes in an orthorhombic system with space group *Fdd2*. Key structural parameters and refinement statistics are provided in Table 1, while the three-dimensional molecular structure is visualized in Figure 2.

Table 1. Crystallographic and refinement data for HDAPYSAC

Crystal data	
Chemical formula	$C_{12}H_{12}N_4O_3S$
Formula weight	292.32
Crystal system, space group	Orthorhombic, *Fdd2*
Temperature (K)	293
a, b, c (Å)	50.121 (4), 14.2546 (8), 7.3490 (4)
V (Å^3)	5250.5 (6)
Z	16
Radiation type	MoKα
μ (mm^{-1})	0.26
Crystal size (mm)	0.35 × 0.29 × 0.21
Data collection	
Diffractometer	STOE IPDS 2
Absorption correction	Integration (X-RED32; Stoe & Cie, 2002)
T_{min}, T_{max}	0.891, 0.971
No. of measured, independent, and observed [I > 2σ(I)] reflections	9081, 2563, 2333
R_{int}	0.069
(sin θ/λ)max (Å^{-1})	0.617
Refinement	
R[F^2 > 2σ(F^2)], wR(F^2), S	0.036, 0.097, 1.06
No. of reflections	2563
No. of parameters	187
No. of restraints	1
H-atom treatment	H atoms treated by a mixture of independent and constrained refinement
$\Delta\rho_{max}$, $\Delta\rho_{min}$ (e Å^{-3})	0.20, −0.16
Absolute structure	Refined as an inversion twin.
Absolute structure parameter	0.03 (11)

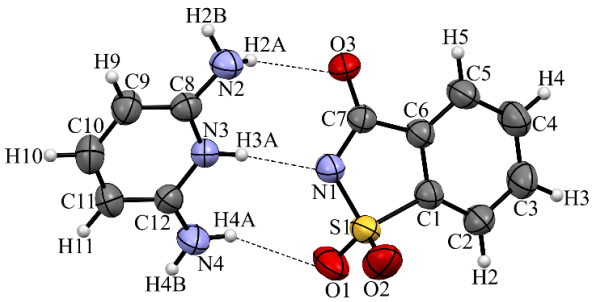

Figure 2. The single crystal structure (ORTEP) of HDAPYSAC

The geometric structure of HDAPYSAC optimized by using DFT at B3LYP/6-311G (d,p) level is shown in Figure 3.

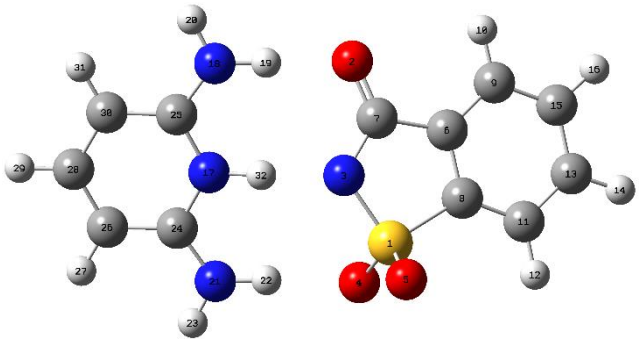

Figure 3. Optimized structure of HDAPYSAC

A comparison of the key geometric parameters obtained from DFT calculations and experimental X-ray data is summarized in Table 2 and Table 3.

Table 2. The optimized and experimental selected bond length of the compound

Bond length (A˚)	XRD	DFT
S1–O1	1.435(3)	1.4351
C2–C3	1.389(5)	1.39
S1–O2	1.441(3)	1.4406
S1–N1	1.613(3)	1.6123
S1–C1	1.770(3)	1.77
C7–C6	1.494(4)	1.4932
N3–C12	1.363(4)	1.3636
N3–C8	1.357(4)	1.3571
C7–O3	1.240(4)	1.2405
N1–C7	1.349(4)	1.3481
N4–C12	1.333(5)	1.3329
N2–C8	1.336(4)	1.3368

Table 3. The optimized and experimental selected bond angles of the compound

Bond angles (°)	XRD	DFT
O1–S1–O2	114.97(18)	114.9686
O1–S1–N1	110.42(17)	110.4346
O2–S1–N1	110.65(17)	110.6535
O1–S1–C1	111.98(17)	111.9581
O2–S1–C1	110.70(18)	110.7134
C12–N3–C8	124.4(3)	124.3672
C7–N1–S1	111.9(2)	111.883
N2–C8–N3	116.9(3)	116.8626
N4–C12–N3	117.2(3)	117.1784
O3–C7–N1	123.2(3)	123.1717
N1–S1–C1	96.66(14)	96.6446

A high level of agreement was observed between the DFT-optimized geometry and the X-ray diffraction results, with only minimal differences attributed to the differing physical states—gas phase for DFT and solid state for XRD. In the saccharin moiety, the S1–O1 and S1–O2 sulfonyl bond lengths were measured as 1.435(3) Å and 1.44(3) Å, respectively, which align closely with those reported for structurally similar sulfonyl compounds [24]. The carbonyl bond (O3–C7) of the benzothiazole group was found to be 1.240(4) Å. A notable deviation was observed in the S1–N1–C7 bond angle (111.9(2)°), which is smaller compared to the 115.0(2)° previously reported [24]. The angles between atoms within conjugated systems, such as N–C–C, N–C–N, O–C–C, and C–N–C, were approximately 120°, a feature typically associated with π-electron delocalization in aromatic systems [21]. Furthermore, the dihedral angle between the benzothiazole ring (C1–C7/N1/S1) and the pyridine ring (C8–C12/N3) was calculated to be 32.810(1)°.

Within the crystalline lattice, intermolecular interactions are established via N4–H4B···O3^{ii} hydrogen bonding, where the pyridinium NH moiety donates a hydrogen bond to the carbonyl oxygen atom. These interactions organize the molecules into C(5) hydrogen-bonded chains aligned along the crystallographic b-axis (Figure 4, Table 4).

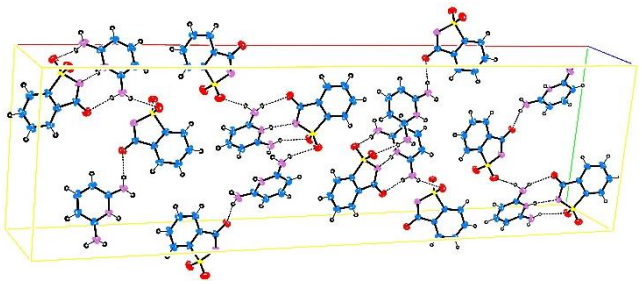

Figure 4. Crystal packing diagram illustrating the intra- and intermolecular hydrogen bonding interactions present in the HDAPYSAC structure

Table 4. Geometric parameters of hydrogen bonds observed in the HDAPYSAC compound

D—H···A	D—H	H···A	D···A	D—H···A
N2—H2A···O3	0.86	2.26	3.032(4)	149.8
N2—H2B···O2^{i}	0.86	2.34	3.151(4)	157.6
N4—H4A···O1	0.86	2.33	3.133(4)	156.5
N4—H4B···O3^{ii}	0.86	2.03	2.879(3)	169.1
N3—H3A···N1	0.82(4)	2.00(4)	2.818(4)	173(4)

Symmetry codes: (i) −x+3/4, y+1/4, z−1/4; (ii) x, y−1/2, z−1/2.

Hydrogen bonding interactions involving N2–H2B ···O2^{i} link the pyridinium NH group to the sulfonyl oxygen of an adjacent molecule, resulting in the formation of C(5) motifs aligned along the crystallographic a-axis. Furthermore, the supramolecular framework is reinforced through additional hydrogen bonds, including N2—H2A···O3 and N3—H3A···N1, which organize the structure into extended chains parallel to the a-axis and give rise to characteristic $R_2^2(8)$ ring patterns. A similar ring motif is also generated by N4—H4A···O1 and N3—H3A···N1 hydrogen bonds, contributing to the overall three-dimensional connectivity.

The HS were generated using a high-resolution setting, with the three-dimensional maps visualized on a fixed color scale ranging from red, indicating shorter-than-expected intermolecular contacts, to blue, indicating longer contacts. This scale spans from –0.5602 to 1.4171 arbitrary units (a.u.). The mapped surface for the HDAPYSAC molecule is shown in Figure 5a. The pale red regions indicate short contacts, primarily associated with N···H···O and N···H···S interactions (Table 2). Figure 5b illustrates the shape index map, generated over the range of –1 to 1 Å. The absence of adjacent red and blue triangle patterns suggests that π–π interactions are not present in the structure. Figure 5c displays the curvedness map in the range of –4.0 to 0.4 Å, where large green areas indicate relatively flat regions on the surface, while blue zones correspond to areas with greater curvature.

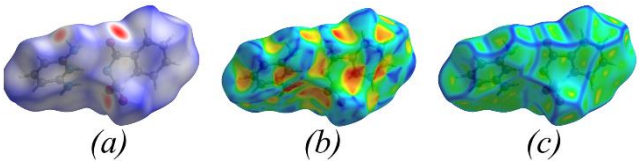

Figure 5. Hirshfeld surface analyses of HDAPYSAC: **(a)** $_{dnorm}$ mapping showing N–H···O and N–H···S short contacts, **(b)** shape index map indicating absence of π–π interactions, and **(c)** curvedness map displaying flat and curved regions.

Figure 6a–g illustrates the Hirshfeld surface mapped with the d_{norm} function, highlighting the intermolecular interactions of H···H, H···O/O···H, H···C/C···H, H···N/N···H, C···C, C···O/O···C, and C···N/N···C, respectively.

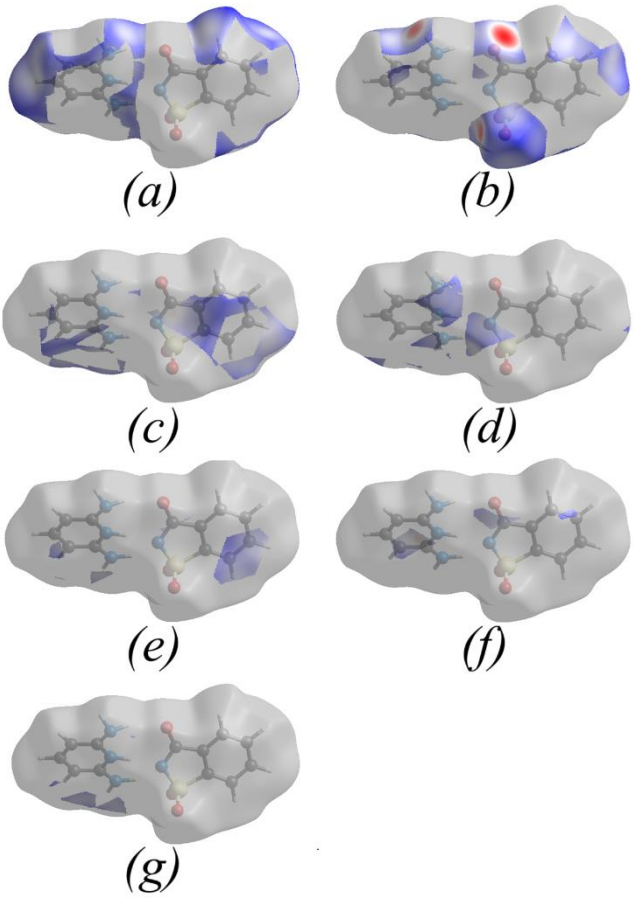

Figure 6. Hirshfeld surface mapped with the d_{norm} function illustrating specific intermolecular interactions: **(a)** H···H, **(b)** H···O/O···H, **(c)** H···C/C···H, **(d)** H···N/N···H, **(e)** C···C, **(f)** C···O/O···C, and **(g)** C···N/N···C contacts.

The comprehensive two-dimensional fingerprint plots, including those segmented by interactions such as H···H, H···O/O···H, H···C/C···H, H···N/N···H, C···C, C···O/O···C, and C···N/N···C, are presented in Figure 7a–h, respectively.

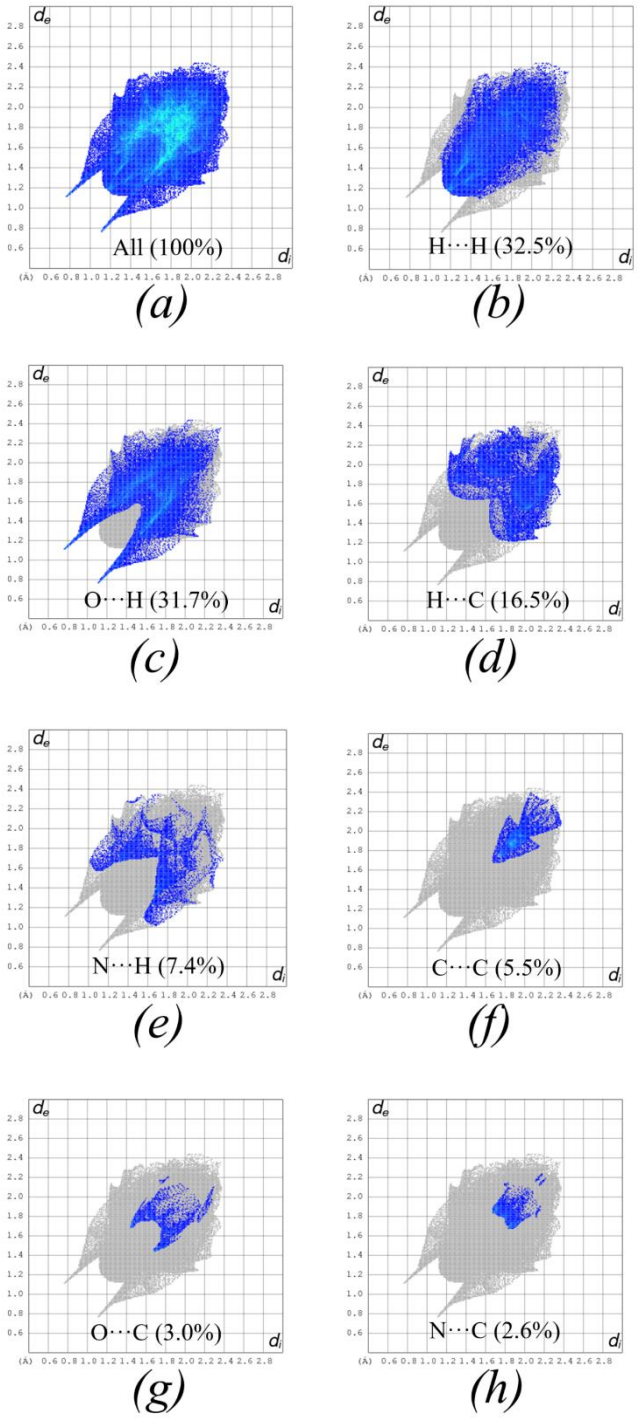

Figure 7. Two-dimensional fingerprint plots of HDAPYSAC: **(a)** overall interactions and breakdown into **(b)** H···H, **(c)** H···O/O···H, **(d)** H···C/C···H, **(e)** H···N/N···H, **(f)** C···C, **(g)** C···O/O···C, and **(h)** C···N/N···C interactions.

The crystal packing is predominantly influenced by H···H interactions, which constitute 32.5% of the Hirshfeld surface area. This is indicated by a central peak at de = di = 1.18 Å in the fingerprint plot. Close behind, H···O/O···H contacts contribute 31.7% and are characterized by a pair of sharp spikes near de + di ≈ 1.85 Å. These interactions primarily result from N—H···O type hydrogen bonds between adjacent molecules (Table 4). Other notable contributions to the

HS analysis indicates that the crystal packing also involves H···C/C···H (16.5%), H···N/N···H (7.4%), C···C (5.5%), C···O/O···C (3.0%), and C···N/N···C (2.6%) intermolecular contacts.

3.2. Frontier Molecular Orbitals (FMOs)

Frontier molecular orbitals, particularly the highest occupied molecular orbital (HOMO) and the lowest unoccupied molecular orbital (LUMO), are essential in defining the optical behavior, electronic characteristics, chemical reactivity, and kinetic stability of molecules. While the HOMO serves as the electron donor, the LUMO acts as the electron acceptor. To deepen the understanding of HDAPYSAC's electronic structure, a frontier molecular orbital analysis was conducted at the B3LYP/6-311G(d,p) theoretical level. Figure 8 presents the graphical depictions of the HOMO and LUMO orbitals.

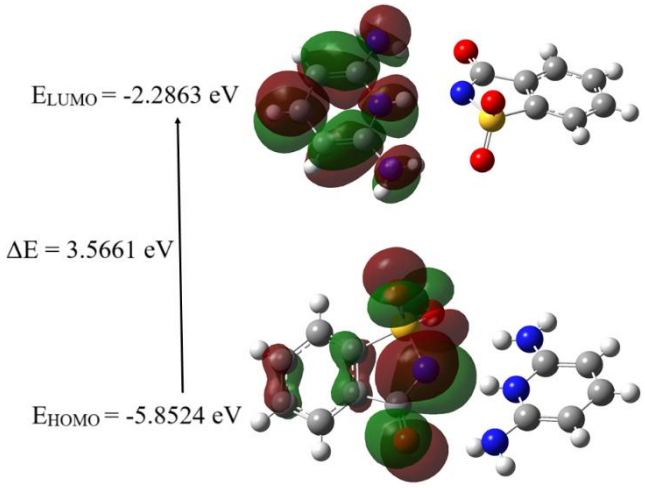

Figure 8. HOMO and LUMO surface plots of the HDAPYSAC molecule obtained from frontier molecular orbital (FMO) analysis

A small energy gap suggests high molecular polarizability and increased chemical reactivity. Table 5 presents a summary of global reactivity descriptors, which include important parameters such as ionization potential (I), electron affinity (A), electronegativity (χ), chemical potential (μ), global hardness (η), global softness (σ), and electrophilicity index (ω). These descriptors are vital for assessing the chemical reactivity of the molecule.

Table 5. The frontier molecular orbitals of HDAPYSAC

FMO	Energy (eV)
E_{HOMO}	-5.8524
E_{LUMO}	-2.2863
Energy difference (ΔE)	3.5661
Ionization Potential (IP)	5.8524
Electron Affinity (EA)	2.2863
Chemical Potential (μ)	-4.0695
Electronegativity (χ)	4.0695
Global Hardness (η)	1.7831
Global Softness (σ)	0.2804
Electrophilicity index (ω)	4.6438

Chemical hardness and softness are indicators of a molecule's stability. These characteristics can be inferred from the HOMO–LUMO energy gap. A large gap suggests that the molecule is hard, while a small gap indicates softness. Soft molecules are generally more polarizable, as they require less energy for electronic excitation. With a HOMO–LUMO gap of 3.5661 eV, the HDAPYSAC molecule can be considered chemically hard.

3.3. Mulliken Atomic Charges

Atomic charges are commonly used to interpret molecular characteristics such as dipole moment, polarizability, electron distribution, and charge transfer behavior. According to the results obtained from DFT diffuse function analysis, atoms H7, H8, H11, H12, H18, H21, H23, H25, and H27 possess positive charges. Hydrogen atoms with positive partial charges may also act as acceptor sites, as indicated in Table 6.

Table 6. Mulliken atomic charges of HDAPYSAC

Atoms	B3LYP/6-311G(d,p)	Atoms	B3LYP/6-311G(d,p)
S1	1.041740	C17	-0.194525
O2	-0.434499	H18	0.096846
N3	-0.413853	C19	-0.199436
N4	-0.670966	C20	0.057445
O5	-0.555582	H21	0.104605
N6	-0.310223	C22	-0.181740
H7	0.206642	H23	0.097620
H8	0.205444	C24	-0.004611
O9	-0.498025	H25	0.083422
N10	-0.413007	C26	0.001095
H11	0.261969	H27	0.095141
H12	0.237757	C28	-0.069659
C13	0.461533	H29	0.088908
C14	0.337072	C30	-0.078576
C15	-0.169324	H31	0.087793
C16	0.435995	H32	0.293000

According to the DFT method and basis set employed for atomic charge analysis, carbon atoms C15, C17, C19, C22, C24, C28, and C30 carry notable negative charges, indicating their role as electron-donating sites. But the charges of C13, C14, C16, C20, and C26 are positive, which are acceptor atoms (Table 6). In addition, positive charges are collected on the S1 atom while negative charges are collected on the O2, N3, N4, O5, N6, O9, and N10 atoms.

3.4. Infrared Spectra

The IR spectrum of the compound shows distinct absorption bands that correspond to the functional groups of its constituent ions. Broad and intense bands observed at 3382 and 3152 cm^{-1} are attributed to the antisymmetric and symmetric N–H stretching vibrations of the 2,6-diaminopyridinium ion, respectively, with some overlap between them. Sharp peaks at 1666 and 1651 cm^{-1} correspond to the carbonyl stretching vibrations of the saccharinate anion. Strong absorption bands around 1261 and 1138 cm^{-1} are assigned to the sulfonyl group vibrations of the saccharinate moiety. Very sharp bands at 1323 and 952 cm^{-1} are related to the symmetric and antisymmetric stretching modes of the CNS group within the saccharinate anion. A summary of the main IR absorption peaks is given in Table 7.

Table 7. Key absorption peaks in the IR spectra of the compound[a] (wavenumber in cm^{-1})

Compound	ν(NH)	ν(CH)	ν(C=O)	$\nu_{asym}(SO_2)$	$\nu_{sym}(SO_2)$	ν_{sym}(CNS)	ν_{asym}(CNS)
(hdapy)(sac)	3382vs 3152vs	3066w 2990w 2851w	1666vs, 1651vs	1261vs	1138vs	1323m	952s

[a] w= weak; vw= very weak; m= medium; s= strong; vs= very strong.

3.5. Ultraviolet Visible Spectral Analysis

The UV-Vis absorption characteristics of the compound were theoretically examined by employing time-dependent density functional theory (TD-DFT) at the B3LYP/6-311G(d,p) computational level, based on the molecule's optimized geometry. The key electronic excitations, along with their corresponding peak wavelengths (λ_{max}), excitation energies, and oscillator strength values, are summarized in Table 8.

Table 8. Summary of excitation energy (cm^{-1}), oscillator strength (f_{os}), and maximum absorption wavelength (λ_{max} in nm) for the HDAPYSAC compound

λ(nm)	E(cm^{-1})	f	Major contributions (>%10)
276.33	36188	0.1592	H-4→LUMO (89%), H-10→L+1 (2%), HOMO→L+2 (4%)
211.26	47335	0.2049	H-4→L+1 (82%), H-12→LUMO (7%), H-10→LUMO (6%)
200.10	49975	0.2188	H-7→L+2 (15%), H-6→L+1 (24%), H-6→L+3 (10%), H3→L+2 (17%), H-2→L+3 (25%), H-5→L+3 (2%)
173.21	57733	0.1679	H-9→L+2 (16%), H-8→L+3 (50%), H-6→L+3 (7%), H-3→L+2 (2%), H-3→L+5 (2%), H-2→L+3 (3%), H-1→L+5 (3%), HOMO→L+4 (6%)
164.35	60846	0.4705	H-12→LUMO (83%), H-11→LUMO (4%), H-4→L+1 (8%)
163.62	61117	0.4882	H-10→L+1 (52%), HOMO→L+5 (19%), HOMO→L+6 (10%), H-9→L+3 (5%)

Two strong absorptions are located at 276.33 and 211.26 nm in the UV-spectrum. The energies of these absorption bands are calculated as 36188, and 473.35 cm^{-1}, respectively. Figure 9 presents a comparison between the experimentally obtained and theoretically predicted UV–vis spectra of the molecule under study.

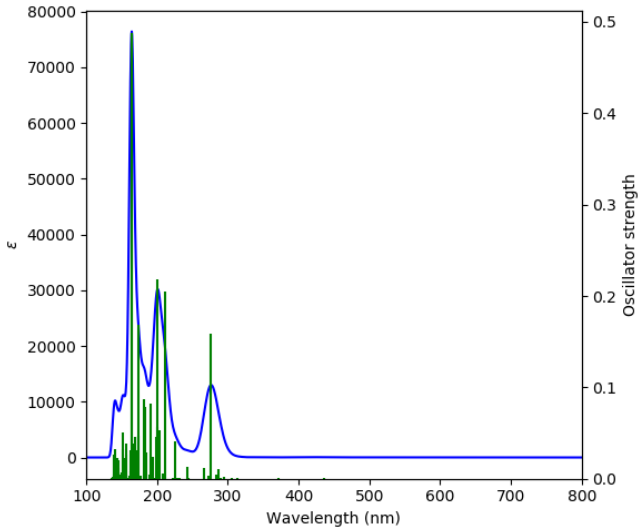

Figure 9. Comparison of calculated and experimental UV–Vis spectra of the HDAPYSAC molecule

The major contributions to the excitation at 276.33 nm originate from the transitions of H-4→LUMO, H-10→L+1, and HOMO→L+2, which correspond to approximately 89%, 2%, and 4%. The excitation at 276.33 nm originates from H-4→L+1, H-12→LUMO, and H-10→LUMO, which correspond approximately 82%, 7% and 6% respectively.

4. Conclusions and Recommendations

In this study, a novel saccharin derivative, 2,6-diaminopyridinium saccharinate ($C_{12}H_{12}N_4O_3S$), was synthesized and its structure was elucidated by FT-IR, UV–vis spectroscopy, and single-crystal X-ray diffraction analysis. The compound was found to crystallize in the orthorhombic system, belonging to the *Fdd2* space group, with unit cell parameters a = 50.121(4) Å, b = 14.2546(8) Å, c = 7.3490(4) Å, and Z = 16. Computational studies on HDAPYSAC were conducted at the DFT/B3LYP/6–311G(d,p) level of theory. Frontier molecular orbital energies were calculated, revealing an energy gap of 3.5661 eV. Mulliken population analysis was employed to determine the atomic charges. Hirshfeld surface analysis and fingerprint plots were utilized to investigate hydrogen bonding and intermolecular interactions in HDAPYSAC. The analysis showed that the crystal packing is mainly governed by H···H (32.5%), H···O/O···H (31.7%), H···C/C···H (16.5%), H···N/N···H (7.4%), C···C (5.5%), C···O/O···C (3.0%), and C···N/N···C (2.6%) contacts. These intermolecular interaction patterns suggest that HDAPYSAC may serve as a promising building block in supramolecular chemistry. Furthermore, the stable molecular framework and hydrogen-bonding features highlight its potential applicability in the design of functional organic–inorganic materials.

Ethics in Publishing

There are no ethical issues regarding the publication of this study.

Acknowledgements

This study has been financed by the Scientific Research Projects Commission of Ordu University (Project number: AR-1650).

References

[1] Baran, E. J., Yılmaz, V. T. (2006). Metal complexes of saccharin. Coord. Chem. Rev., 250(15-16), 1980-1999.

[2] Kaur, K., Srivastava, S. (2020) Artificial sugar saccharin and its derivatives: role as a catalyst. RSC Adv., 10(60), 36571-36608.

[3] İçsel, C., Yılmaz, V. T., Yeşilel, O. Z., Harrison. V. T. A. (2024). Metal complexes of saccharin and thiosaccharin as potential anticancer and antimicrobial agents. Eur. J. Med. Chem. Rep., 12, 100205.

[4] Jovanovski, G., Grupče, O., Šoptrajanov, B. (1990). The O-H and O-D stretching vibrations in the hydrates of sodium and potassium saccharinate: spectra-structure correlations. J. Mol. Struct., 219, 61-66.

[5] Jovanovski, G., Kaitner, B., Grupce, O., Naumov, P. (2004). Crystal structure, infrared and raman spectra of tripotassium trisaccharinate dihydrate, $K_3(C_7H_4NO_3S)_3 \cdot 2H_2O$. Cent. Eur. J. Chem., 2(1), 254-275.

[6] Jovanovski, G., Kamenar, B. (1982). Two ionic saccharinates:(la) sodium saccharinate 2/3 hydrate, $C_7H_4NO_3SNa \cdot 2/3H_2O$;(lb) Magnesium disaccharinate heptahydrate, $(C_7H_4NO_3S)_2Mg \cdot 7H_2O$. Cryst. Struct. Commun., 11, 247–255.

[7] Ng, S. W. (1998). Ammonium saccharin. Acta Crystallogr. Sect. C: Cryst. Struct. Commun., 54(5), 649-651.

[8] Gümüş, S., Güney, S., Yılmaz, V. T., Kazak, C. (2006). A Non-Metallic Ionic Saccharinate. Synthesis, Structure and DFT Calculations of Piperazinium Disaccharinate. Zeitschrift für anorganische und allgemeine Chemie, 632, 1544-1548.

[9] Bouaziz, E., Hassen, C. B., Chniba-Boudjada, N., Daoud, A., Mhiri, T., Boujelbene, M. (2017). Crystal structure, Hirshfeld surface analysis, vibrational, thermal behavior and UV spectroscopy of (2, 6-diaminopyridinium) dihydrogen arsenate. J. Mol. Struct., 1145, 121-131.

[10] Hassen, C. B., Dammak, T., Chniba-Boudjada, N., Mhiri, T., Boujelbene, M. (2017). Chemical synthesis, crystal structure, vibrational spectroscopy, non-linear optical properties and DFT calculation of bis (2, 6-diaminopyridinium) sulfate monohydrate. J. Mol. Struct., 1127, 43-52.

[11] Fredj, D., Hassen, C. B., Elleuch, S., Feki, H., Boudjada, N. C., Mhiri, T., Boujelbene, M. (2017). Structural, vibrational and optical properties of a new organic–inorganic material:$(C_5H_8N_3)_2[BiCl_5]$. Mater. Res. Bull. 85, 23-29.

[12] Li, B., Yu, Y., Xin, M., Xu, J., Zhao, T., Kang, H., Xing, G., Zhao, Zhang, T., Jiang, S. (2023). Second-order nonlinear optical properties of copper-based hybrid organic–inorganic perovskites induced by chiral amines. Nanoscale, 15(4), 1595-1601.

[13] Majhi, S. M., Ali, A., Rai, P., Greish, Y. E., Alzamly, A., Surya, S. G., Qamhieh, N., Mahmoud, S. T. (2022). Metal–organic frameworks for advanced transducer based gas sensors: review and perspectives. Nanoscale Advances, 4(3), 697-732.

14. Sun, P., Wang, Y., Li, Z., Guo, H., Yin, X., Pei, H. (2020). A flexible organic–inorganic hybrid for medium-temperature proton conduction over a wide humidity range. Journal of Materials Science, 55(27), 13075-13084. https://doi.org/10.1007/s10853-020-04984-x

[15] Kanmazalp, S. D., Sagher, M., Dege, N., Içbudak, H. (2023). Synthesis, hirshfeld surface, ftir analysis and single crystal X-ray structure of 2-amino-3-hydroxypyridinium saccharinate. J. Struct. Chem., 64(6), 1137-1146.

[16] Haider, S. Z., Malik, K. M. A., Das, S., & Hursthouse, M. B. (1984). zinc (II) Dihydrate, $[Zn(C_7H_4NO_3S)_2\ (H_2O)_4]\cdot 2H_2O$, and Tetraaquabis (saccharinato-N) cadmium (II) Dihydrate, $[Cd(C_7H_4NO_3S)_2(H_2O)_4]\cdot 2H_2O$. Acta Crystallogr., C, 40, 1147-1150.

[17] Stoe & Cie (2002) X-AREA and X-RED32, Stoe & Cie GmbH, Darmstadt (Germany).

[18] Sheldrick, G. M. (2015). Crystal structure refinement with SHELXL. Acta Cryst., C71, 3–8.

[19] Macrae, C. F., Edgington, P. R., McCabe, P., Pidcock, E., Shields, G. P., Taylor, R., Towler, M., van de Streek, J. (2006). Mercury: visualization and analysis of crystal structures. J. Appl. Crystallogr., 39(3), 453-457.

[20] Spek, A. L. (2003). Single-crystal structure validation with the program PLATON. J. Appl. Crystallogr., 36(1), 7-13.

[21] Farrugia, L.J. (1999). WinGX suite for small-molecule single-crystal crystallography. J. Appl. Crystallogr. 32, 837–838.

[22] Westrip, S. P. (2010). publCIF: software for editing, validating and formatting crystallographic information files. J. Appl. Crystallogr., 43, 920–925.

[23] Frisch, M. J., Trucks, G. W., Schlegel, H. B., Scuseria, G. E., Robb, M. A., Cheeseman, J. R., Scalmani, G., Barone, V., Mennucci, B., Petersson, G. A., Nakatsuji, H., Caricato, M., Li, X., Hratchian, H. P., Izmaylov, A. F., Bloino, J., Zheng, G., Sonnenberg, J. L., Hada, M., Ehara, M., Toyota, K., Fukuda, R., Hasegawa, J., Ishida, M., Nakajima, T., Honda, Y., Kitao, O., Nakai, H., Vreven, T., Montgomery Jr, J. A., Peralta, J. E., Ogliaro, F., Bearpark, M., Heyd, J.

J., Brothers, E., Kudin, K. N., Staroverov, V. N., Keith, T., Kobayashi, R., Normand, J., Raghavachari, K., Rendell, A., Burant, J. C., Iyengar, S. S., Tomasi, J., Cossi, M., Rega, N., Millam, J. M., Klene, M., Knox, J. E., Cross, J. B., Bakken, V., Adamo, C., Jaramillo, J., Gomperts, R., Stratmann, R. E., Yazyev, O., Austin, A. J., Cammi, R., Pomelli, C., Ochterski, J. W., Martin, R. L., Morokuma, K., Zakrzewski, V. G., Voth, G. A., Salvador, P., Dannenberg, J. J., Dapprich, S., Daniels, A. D., Farkas, O., Foresman, J. B., Ortiz, J. V., Cioslowski, J., Fox, D. J. (2010). Gaussian 09, Revision C.01, Gaussian, Inc, Wallingford C.p*ooo-iokı7

[24] Dennington, R., Keith, T., Millam, J. (2010). GaussView, Version 5, Semichem Inc, Shawnee Mission KS.

[25] Becke, A. D. (1988). Density-functional exchange-energy approximation with correct asymptotic behavior. Phys. Rev., A 38, 3098.

[26] Lee, C., Yang, W., Parr, R. G. (1988). Development of the Colle-Salvetti correlation-energy formula into a functional of the electron density. Physical review, B 37, 785.6

[27] Turner, M. J., MacKinnon, J. J., Wolff, S. K., Grimwood, D. J., Spackman, P. R., Jayatilaka, D., Spackman, M. A. (2017). Crystal Explorer Version 17.5, University of Western Australia.